Theory of Microphase Segregation in ABA Triblock Comb-Shaped Copolymers: Lamellar Mesophase

Ivan Mikhailov, Frans Leermakers, Anatoly Darinskii, Ekaterina Zhulina, Oleg Borisov

Theory of microphase segregation in ABA triblock comb-shaped copolymers: lamellar mesophase

Ivan V.Mikhailov[1], Frans A.M. Leermakers[2], Anatoly A. Darinskii[1], Ekaterina B. Zhulina[1], Oleg V. Borisov[3,1*]

[1]Institute of Macromolecular Compounds of the Russian Academy of Sciences, St.Petersburg, Russia,

[2]Physical Chemistry and Soft Matter, Wageningen University, 6703 NB Wageningen, The Netherlands,

[3]Institut des Sciences Analytiques et de Physico-Chimie pour l'Environnement et les Matériaux, UMR 5254 CNRS UPPA, Pau, France

April 5, 2021

email: oleg.borisov@uiv-pau.fr

For Table of Contents Use Only

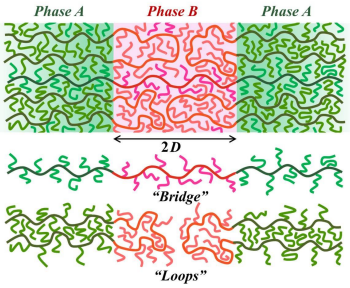

"Theory of microphase segregation in ABA triblock comb-shaped copolymers: lamellar mesophase"

Authors: Ivan V.Mikhailov, Frans A.M. Leermakers, Anatoly A. Darinskii, Ekaterina B. Zhulina, Oleg V. Borisov.

Abstract

Theory describing lamellar mesophases formed in the melt of ABA triblock copolymers with strongly incompatible comblike blocks is developed using combination of strong-stretching self-consistent field (SS-SCF) analytical approach and numerical self-consistent field calculations based on the Scheutjens-Fleer (SF-SCF) methods. Structural and thermodynamic properties of the lamellae are analysied as a function of architectural parameters, i.e. grafting density and polymerization degree of the main and side chains in the comb-shaped blocks. In particular, we distinguish between loops and bridges formed by middle comb-shaped block and demonstrate how fraction of bridges connecting neighboring AB interfaces of the lamellar layers and shear modulus of the mesophase are mediated by architectural parameters of comblike blocks. In particular, we predict an increase in the shear modulus upon replacement of linear ABA triblock copolymers by comblike ones with the same composition. The asymptotic analytical predictions of the theory are complemented by the results of numerical modelling.

1 Introduction

Brushes of branched polymers became a subject of intense theoretical investigation during the last decade.[1–7] Solvated or dry brushlike structures arise, e.g., upon self-assembly of block copolymers with branched blocks in selective solvent[8–12] or in the melt state.[13–22]

An interest to covalently-linked to the surface or self-assembled brushes of branched macromolecules is motivated by applications in nanomedicine, particularly for drug and gene delivery systems[12] and antifouling surfaces[23–25] due to the increased number of potentially functionalized and exposed to the environment free ends. On the other hand, microphase segregated bulk morphologies of block copolymers with branched blocks exhibit specific mechanical properties that facilitate the design of novel biomimetic, including tissue-like materials.[26–29]

It was recently realized that structural properties of brushes formed by end-tethered polymers with certain branched architectures (e.g., regular dendrons, arm-tethered stars, etc.) can be described by means of the analytical theory incorporating architecture-dependent self-consistent molecular potential. The pioneering study of Pickett[1] demonstrated a parabolic nature of the self-consistent molecular potential acting in brushes formed by strongly stretched root-tethered regular dendrons and paved the way to generalization of this analytical approach to other molecular architectures.[30–34]

In our recent study[35] we applied the parabolic potential framework (refered to as SS-SCF approach) to study microphase segregated melts of AB diblock copolymers with blocks composed of molecular brushes (comb-shaped polymers). In the strong segregation limit, the domain- and matrix-forming blocks of such macromolecules could be modelled as tethered to A/B interfaces constituting solvent-free brushes of comblike/bottlebrush polymers. In this paper we extend the analysis to lamellar mesophases formed by triblock ABA copolymers comprising comblike blocks. In contrast to diblock macromolecules, triblock copolymers organize in domains interconnected by the central (bridging) blocks of these macromolecules. That is, some of the central blocks in microphase segregated melts form loops by returning to the same domain, while others make bridges connecting the neighboring domains (**Figure 1**). The fraction of bridges is an important characteristics of the system because it controlls shear modulus of the lamellar structure. By using the parabolic potential SS-SCF framework and the numerical SF-SCF modeling we analyze here how the equilibrium fraction of bridges in lamellar mesophase and its shear modulus are governed and can be tuned by variable architectural parameters of ABA triblock copolymer.

The rest of the paper is organized as follows. In Section 2 we outline

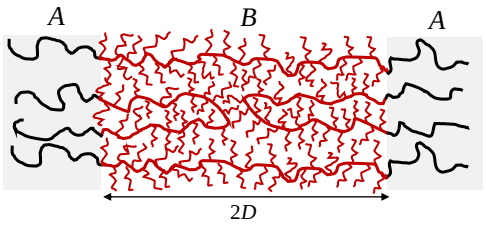

Figure 1: Schematics of lamellar mesophase formed by ABA triblock copolymers with comb-shaped central B-blocks.

the basic elements of the analytical self-consistent field (SS-SCF) and the numerical (SF-SCF) approaches and briefly review the results obtained in ref[36] for solvent-free brushes formed by comblike macromolecules tethered by one end of the main chain to an impermeable interface. In Section 3 we calculate the equilibrium fractions of loops and bridges in solvent-free brushes formed by comb-shapes macromolecules with both main chain ends tethered to any of two apposing grafting surfaces and compare abalytical results with the results of numerical SF-SCF calculations. In Section 4 we use the obtained results for analysing structural and mechanical properties of lamellar mesophases formed by ABA triblock copolymers with comb-shaped B-blocks and analyze dependence of fraction bridging B-blocks and shear modulus on the set of architectural parameters of the comb-shaped blocks. Finally, in Section 6 we formulate our conclusions.

2 Brush of end-tethered comblike macromolecules

Following ref,[36] consider first a solvent-free brush formed by comblike polymers tethered by one end of the main chain to an impermeable planar surface with area s per molecule. Each macromolecule comprises $P \gg 1$ repeats each composed of the backbone spacer with degree of polymerization (DP) m and $q \geq 1$ side chains with n monomer units each, linked to each junction on the backbone, see **Figure 2**. The backbone and side chains are assumed to be chemically identical, and have monomer units with length l, volume υ, and Kuhn segment $b > l$. If $q > 1$, the macromolecules are termed "barbwire" polymers. The backbone has DP $M = Pm$ while the total degree of polymerization of the macromolecule is

$$N = P(m + qn) = M(1 + qn/m) \tag{1}$$

The grafting density $\sigma = 1/s$ ensures strong overlap of individual macromolecules so that the side chains and spacers are extended in the direction normal to the grafting surface with cut-off of polymer density profile (brush thickness) at distance $D = N\upsilon/s$ from the surface.

Following the strong stretching self-consistent field (SS-SCF) approach formulated earlier,[35] the molecular potential $U(z)$ in a solvent-free brush exhibits parabolic dependence as a function of distance z from the grafting surface,

$$\frac{U(z)}{k_B T} = \frac{3}{2lb}\kappa^2(D^2 - z^2) \tag{2}$$

with architecture-dependent topological coefficient κ. The latter depends on DPs of the side chains (n), the backbone spacer (m), the number q of side chains emanating from each branching point and total number (P) of branching units but is remarkably independent of the chain grafting density σ or the brush geometry. Eq 2 presumes the Gaussian (linear) elasticity of the tethered chains on all length scales. That is, the we focus here on comblike polymers with backbones whose Kuhn length is not renormalized by stretching due to the presense of side chains. Crowding of the side chains near the branching points is not taken into account, which imposes a restriction on the branching activity, $q \gtrsim 1$. Another restriction on applicability of eq 2 is possible appearance of the dead zones (depleted of the free ends of backbones), and the chains stratification for certain architectural parameters of comblike polymers. In these cases eq 2 serves as an approximation to be examined by the numerical self-consistent field methods. The applicability of the parabolic potential approximation to any specific branched architecture of the brush-forming molecules can be checked by the numerical

self-consistent methods (e.g., SF-SCF modelling[39]) that are free of any pre-assumption about the shape of the self-consistent molecular potential and do account for finite extensibility of the macromolecules. The basic elements of SF-SCF modeling are described in **SI**.

In our previous publication[36] we have analyzed how the topological coefficient κ depends on architectural parameters of the comb-shaped polymer with $q \geq 1$, i.e., the lengths of side chains and spacers, n and m, and of its backbone, $M = mP$. We demonstrated that for comblike polymers κ exhibits two different asymptotic dependences for polymers with short, $M \ll (nm/q)^{1/2}$, and long, $M \gg (nm/q)^{1/2}$, backbones. In this paper we focus on comblike polymers with long backbones, $M \gg (nm/q)^{1/2}$, which allows us to use the asymptotic power law for the topological coefficient κ,

$$\kappa = \frac{\pi}{2N}\left(1+\frac{qn}{m}\right)^{1/2} = \frac{\pi}{2M}\left(1+\frac{nq}{m}\right)^{-1/2}, \qquad M \gg (nm/q)^{1/2} \tag{3}$$

For linear chains with $q = 0$ and $N = M$, the topological coefficient $\kappa = \kappa_{lin} = \pi/2N$. To eliminate the molecular weight dependence, we introduce the topological ratio

$$\eta = \frac{\kappa}{\kappa_{lin}} = \frac{2\kappa N}{\pi}$$

which is approximated as

$$\eta = \left(1+\frac{qn}{m}\right)^{1/2} \tag{4}$$

for barbwire comblike polymers with $M \gg (nm/q)^{1/2}$. Conventional comblike polymers exhibit $q = 1$.

Equations 3 and 4 provide important insights in the equilibrium structure of solvent-free planar layer formed by end-tethered comblike polymers. They indicate that the elastic free energy of comblike polymers in a brush is dominated by the stretching of the backbone while side chains retain almost unperturbed Gaussian conformations.

As it was demonstrated by means of the numerical SF-SCF calculations,[36] the conformations of backbones in comb-shape polymers (distribution of elastic tension along the chain and distribution of the end segments) are very close to those for linear chains of the same DP forming a solvent-free brush.

3 Central B-domain of the lamella: brush of loops and bridges

To mimic B-domain formed by comblike central blocks of ABA triblock copolymer we consider two apposing solvent-free brushes comprising loops

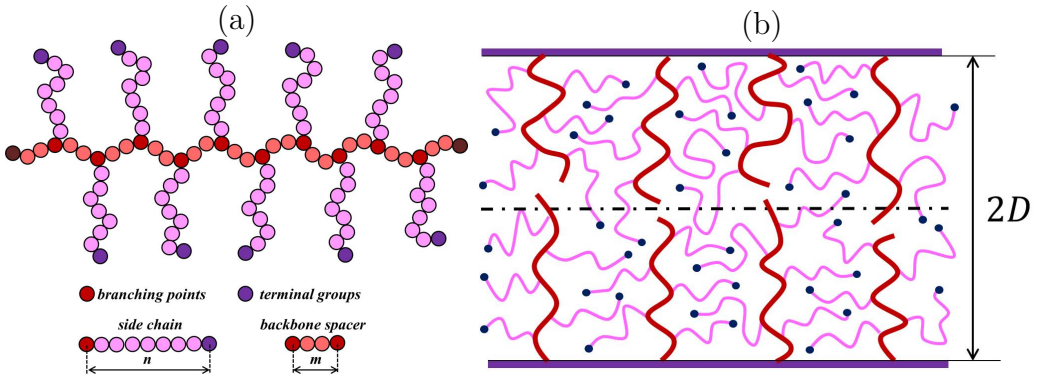

Figure 2: Model of comblike polymer implemented in SF-SCF calculations (a), and schematic of apposing solvent-free planar brushes of comblike polymers (b) The DPs of the main chains, side chains and a spacers of comblike polymers are M, n and $m = M/P$, respectively. The grafting area per macromolecule is s .

(with both main chain ends tethered to the same grafting surface) and bridgies connecting apposing grafting surfaces. The brushes are brought in grazing contact.

Although the average stretching of comblike B-blocks in bridges is larger than that in loops, a non-zero fraction of bridges under thermal equilibrium conditions is due to the gain in mixing entropy of loops and bridges. To specify the equilibrium fraction of bridges in brushes of comblike polymers, we follow the original model developed in ref[37] for solvent-free brushes formed by linear chains and predicting equilibrium fraction X of bridges. A brief review of this model is presented in the following subsection whereas the details of calculations are delegated to **SI**.

3.1 Brush of loops and bridges formed by linear chains

A B-domain formed by central B-blocks in lamellar phase of triblock linear ABA copolymers can be envisioned as consisting of two apposing brushes comprising loops (both chain ends are tethered to the same A/B interface) and bridges connecting apposing AB interfaces, **Figure 3a**.

Let the fraction of chains forming bridges be $0 \leq X \leq 1$. Let the area per chain on one interface be $2s$ and the number of monomer units per chain be $2M$. Then the half distance between A/B interfaces is $D = Mv/s$. If Σ_{AB} is the area of one A/B interface, then total number of chains in two brushes is $2(\Sigma_{AB}/2s) = \Sigma_{AB}/s$, the number of bridges is $X\Sigma_{AB}/s$, and the number of loops is $(1-X)\Sigma_{AB}/s$. The number of loops of return to the same A/B

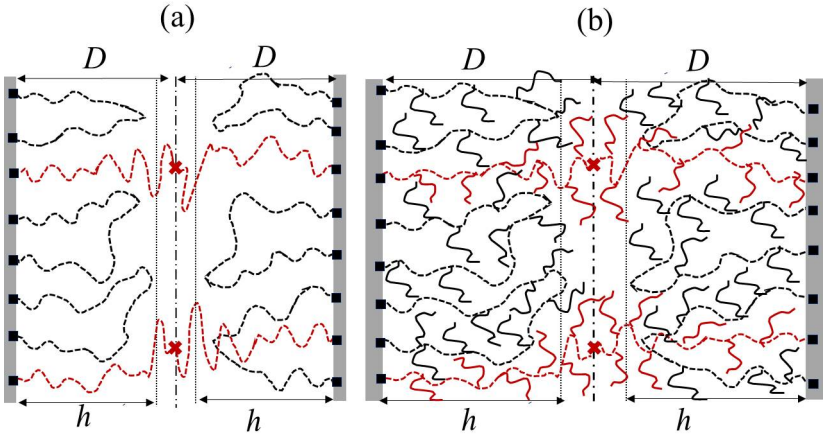

Figure 3: Schematics of two apposing brushes formed by (a) loops and bridges of linear chains of DP $2M$ and (b) comb-like polymers with DPs of the main chains, side chains and spacers $2M$, n and m, respectively. Grafting area per macromolecule is $2s$.

interface is $\frac{1}{2}(1-X)\Sigma_{AB}/s$.

Because of the symmetry of the system, the middle monomer units of bridges are located in average at the middle plane. Two simplifying the analysis assumptions are made: (i) The middle points of bridges are pinned at the middle plane separating the brushes, so that both halves of each bridge (subchains with end-points fixed at symmetry plane between apposing brushes) comprise N monomer units. (ii) Each loop is cut in its middle point and modelled as two end-tethered linear subchains with DP M and uncorrelated positions of the free ends. Hence, half of the B-domain is modelled as a brush of linear chains with grafting area per chain s and DP M, among which $X\Sigma_{AB}/s$ have their terminal monomer unit pinned at $z = D$ ("bridges") and $2\cdot(1/2)(1-X)\Sigma_{AB}/s = (1-X)\Sigma_{AB}/s$ have freely fluctuating ends.

In the framework of the SS-SCF approach, loops and segments of bridges with M' monomer units occupy proximal to A/B interfaces sublayers with thickness $h < D$, and experience parabolic potential (eq 2 with topological coefficient $\kappa = \pi/2N$), which is truncated at $z = h$. The central part of the B-domain, i.e., the layer with thickness $2(D-h)$, comprises only uniformly stretched segments of bridges each comprising $2(N-N')$, monomer units; these monomer units experience constant potential, $U(h)$.

Following ref,[37] we introduce fraction $\tau = (M-M')/M$ of monomer units

of bridges that form central part of the layer, leading to the relationship

$$h/D = 1 - X\tau \tag{5}$$

The elastic free energy F_{el} per subchain in the brush with fraction X of bridges was calculated in ref,[37] and is given by

$$\frac{F_{el,lin}(X)}{k_BT} = \frac{\pi^2}{8}\frac{D^2}{lbM}\left[(1-\tau X)^3 + \frac{12X^2}{\pi^2}\right] = \frac{F_{el,lin}(0)}{k_BT}\left[(1-\tau X)^3 + \frac{12X^2}{\pi^2}\right] \tag{6}$$

with X and τ related as

$$(1-\tau X) = \frac{2X}{\pi}\cot\left(\frac{\pi\tau}{2}\right), \tag{7}$$

and the elastic free energy $F_{el,lin}(0)$ per subchain in the brush with no bridges ($X = 0$),

$$\frac{F_{el,lin}(0)}{k_BT} = \frac{\pi^2}{8}\frac{D^2}{lbM} \tag{8}$$

Obviously, the elastic free energy $F_{el,lin}(X)$ given by eq 6 is an increasing function of X.

However, an option for B-blocks to make either loops or bridges brings an additional combinatorial entropy in the system. The entropy F_{mix} of mixing loops and bridges can be approximated as

$$\frac{F_{mix}}{k_BT} = X\ln X + (1-X)\ln(1-X), \tag{9}$$

Then minimization of the total free energy per chain, $F = F_{el} + F_{mix}$, with respect to X leads to equation for the equilibrium fraction X_B of bridges that with accuracy of $O(X^3)$ reduces to

$$\frac{24}{\pi^2}\frac{D^2}{lbM}X_B^3 + \ln\frac{X_B}{1-X_B} = 0 \tag{10}$$

By expanding eq 10 with respect to $(1/2 - X_B)$, and retaining terms up to $O(X^3)$ one arrives at an expression for X_B,

$$\frac{1-X_B}{X_B} = \left(1 + \frac{9D^2}{\pi^2 lbM}\right)^{1/3} = \left(1 + \frac{72}{\pi^4}\frac{F_{el,lin}(0)}{k_BT}\right)^{1/3}, \tag{11}$$

fraction

$$\tau \approx \frac{4}{\pi^2}X_B \tag{12}$$

of monomer units per bridge in the central region, and thickness

$$h \approx D(1 - \frac{4}{\pi^2} X_B^2) \tag{13}$$

of the proximal to the grafting surface layer. Schematic of a planar layer formed by loops and bridges that lead to eqs. 12,13 and 11 is presented in **Figure 3a**.

As it follows from eqs 11 and 14, the equilibrium fraction X_B of bridges could be estimated from the equilibrium properties of a brush formed by chains with free end-points (linear chains with DP N tethered with area s per chain) as

$$X_B \approx \frac{1}{1 + \left(1 + \frac{72}{\pi^4} \frac{F_{el,lin}(0)}{k_B T}\right)^{1/3}} \tag{14}$$

For strongly stretched chains, $F_{el,lin}(0)/k_BT \gg 1$, the second term in brackets dominates making $X_B \ll 1$, and eq 11 reduces to the previously obtained[37] scaling dependence

$$X_B \simeq \left(\frac{Mlb}{D^2}\right)^{1/3} = \left(\frac{lb}{\upsilon^2 M} s^2\right)^{1/3} \sim (\frac{F_{el,lin}(0)}{k_B T})^{-1/3} \tag{15}$$

Under these conditions, bridging invokes only $O(X_B^4)$ correction to the elastic free energy per subchain (second term in brackets in eq 16),

$$\frac{F_{el,lin}(X_B)}{k_B T} = \frac{F_{el,lin}(0)}{k_B T} \left[1 + \left(\frac{2X_B}{\pi}\right)^4\right] \tag{16}$$

In **Figure 4** we compare the results of the analytical SS-SCF and numerical SF-SCF models for the equilibrium fraction X_B, and the elastic free energy $F_{el,lin}(X_B)$ as a function of the brush thickness D. Dashed lines indicate the theoretical predictions (calculated via eqs 14 and 16), red lines are the results of the SF-SCF numerical model.

As it is seen from **Figure 4**, the analytical and numerical models are in perfect agreement in the range of the system parameters that ensure considerable elongation of the chains with respect to their Gaussian size ($\sim M^{1/2} \approx 10$ for $\mathbf{2}N = 201$) in the linear elasticity regime. Deviations from the theoretical curve for X_B are found upon onset of nonlinear chain elasticity at $D/aM \gtrsim 0.5$.

Overall data for brushes of loops and bridges formed by linear chains indicate a remarkably good correspondence between the analytical and numerical self-consistent field models in the regime of Gaussian elasticity for the brush-forming polymers.

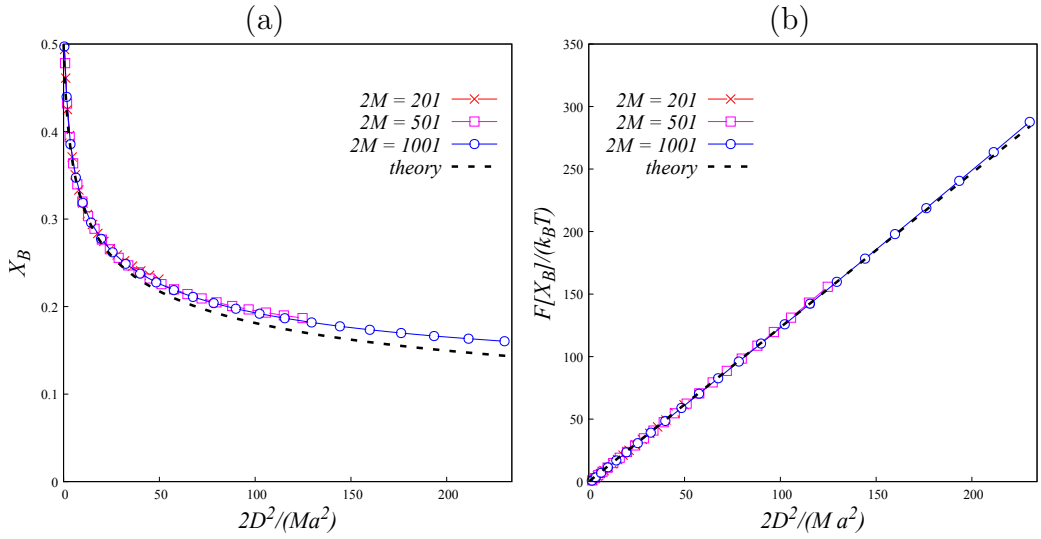

Figure 4: Equilibrium fraction of bridges X_B in planar layers of linear chains (a), and the corresponding free energy per chain (b) measured in k_BT units, as a function of $2D^2/(Ma^2)$.

3.2 Brush of loops and bridges formed by comblike polymers

The corroboration of the analytical predictions by the numerical SF-SCF calculations in the previous section suggests that the layer of loops and bridges formed by comblike polymers with long backbones might retain the structure similar to that for linear chains. That is, the central region filled predominantly by monomer units from the bridges, and the loops localized closer to grafting surfaces. Schematic of a planar brush of loops and bridges formed by comblike polymers is presented in **Figure 3b**.

In **Figure 5** we present typical SF-SCF data for volume fractions $\varphi(z)$ and $\varphi_M(z)$ of monomer units that belong to the side chains in loops (black solid lines) and bridges (red solid lines), and the backbones of loops and bridges (dashed black and red lines, respectively).

As it is seen in **Figure 5**, the basic structure of the layer remains similar to that for linear chains ($n = 0$, **Figure 5a**): monomer units of the backbones of bridges together with their side chains occupy the central region of the layer, while backbones of loops with their side chains dominate in the proximal regions of the layer. The backbones of loops formed by comblike polymers show better segregation than loops of linear chains. As it is also seen in **Figure 5d** which shows a magnified distribution $\varphi_M(z)$ of monomer units of the backbones, backbones of the loops from apposing brushes do not

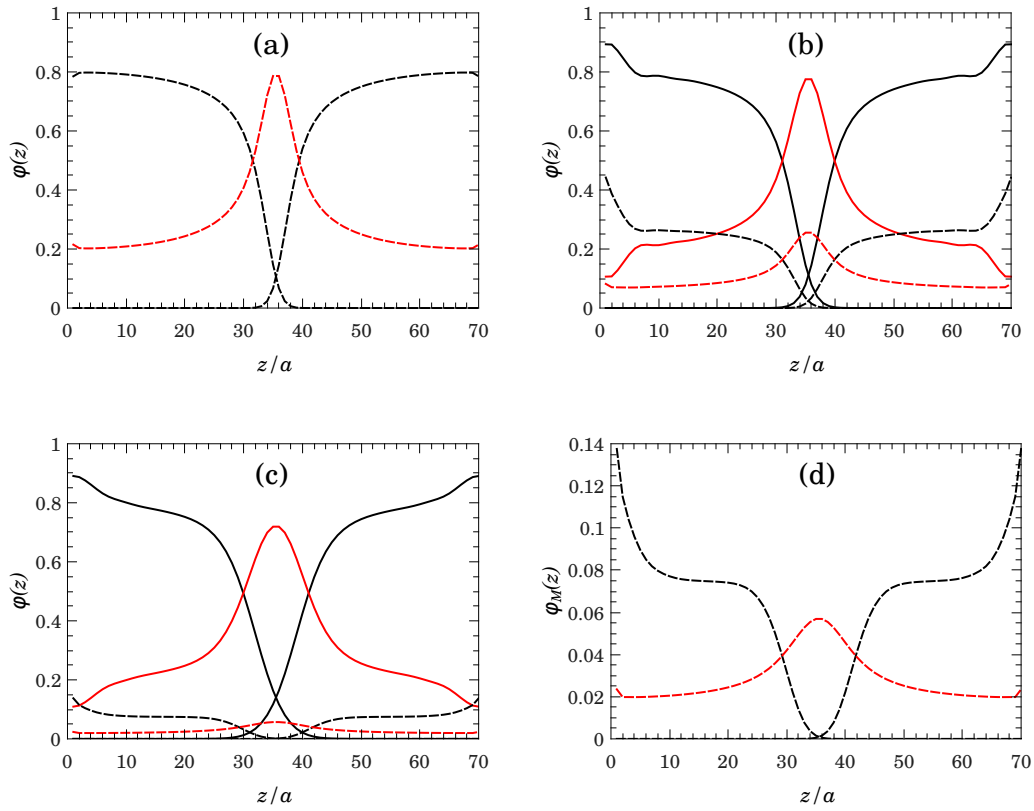

Figure 5: SF-SCF distributions of monomer units from the side chains from loops (solid black lines), loop backbones (dashed black lines), side chains of bridges (solid red lines), and bridge backbones (dashed red lines). Values of parameters $m = 10$, $2M = 201$, $2D/a = 70$, $X = 0.3$, $n = 0$ (a), $n = 20$ (b), $n = 100$ (c). Magnified distributions $\varphi_M(z)$ for backbones of loops and bridges for $n = 100$ are shown in (d).

overlap, compared to limited overlapping of loops by linear chains in **Figure 5a**. Moreover, in contrast to linear chains, the volume fraction $\varphi_M(z)$ of the backbone monomer units in comblike polymers increases near grafting surfaces.

As it follows from SF-SCF data in **Figures 5**, the backbones of loops become less stretched upon increasing n via accumulation of their monomer units near grafting surfaces (see also **Figure 7**). As a result, the sublayers with thickness $\sim an^{1/2}$ in the vicinity of the central region could be depleted of the backbone segments, and contain mostly monomer units of side chains decreasing thereby the average extension of backbones.

To get more insights in the equilibrium structure of brushes formed by comblike polymers, we examined molecular potential $U(z)$ in a solvent-free brush of loops.

In **Figure 6** the dimensionless potential $U(z)/k_BT$ is presented as a function of $(z/a)^2$ for a set of comblike polymers with short spacers $m = 2$ (a) and $m = 4$ (b), fixed $M = 1001$, $2D/a = 300$, and varying DP n of side chains. Straight dashed lines indicate parabolas, triangles mark the theoretical values of potential $U(0)$ calculated according to eqs 2,3,

$$\frac{U(0)}{k_BT} = \frac{3}{2}\kappa^2\left(\frac{D}{a}\right)^2 = \frac{3\pi^2}{8}\left(\frac{D}{aM}\right)^2\frac{1}{(1+n/m)} \tag{17}$$

As it follows from **Figure 6**, the agreement between the numerical SF-SCF and the analytical SS-SCF models is encouraging. Relatively small deviations of the SF-SCF data from the dashed line for linear chains ($n = 0$) are invoked by onset of nonlinear elasticity. An increase in n up to 80 (not shown in **Figure 6**) leads to a better "parabolicity" of $U(z)$. Moreover, in agreement with eq 3 the dependences $U(z)$ in **Figures 6a** ($m = 2$) and **Figure 6b** ($m = 4$) perfectly match each other for equal values of n/m (shown by similar colors).

In **Figures 7** we present volume fractions $\varphi_M(z)$ of the backbone monomer units for a set of comblike polymers with the same parameters as in **Figure 6**. To estimate the increase in φ_M in the vicinity of the grafting surface consider a volume V with area s and width $\sim an^{1/2}$ that contains $p \simeq V/(a^3n) = s/(a^2\sqrt{n})$ side chains with $n \gg m$, originating from the backbone segment with length $pm \simeq sm/(a^2\sqrt{n})$. In the body of the brush the average volume fraction of the backbone monomer units is almost constant, $\varphi_M(z) \approx m/n$, to preserve the unperturbed state of side chains. If pm backbone monomer units are extracted from the vicinity of central domain, and equal amount of monomer units is accomodated within distance $\sim an^{1/2}$ from the grafting surface (the Gaussian size of unperturbed side chain), the

average volume fraction of backbone monomer units would increase there by $\Delta\varphi_M \simeq a^3pm/(asn^{1/2}) \simeq m/n \simeq \varphi_M$. Therefore, the increase in presurface concentration of backbone monomer units yields $\Delta\varphi_M/\varphi_M \simeq 1$, which is consistent with the data in **Figures 5 and 7**.

In **Figures 8** we present normalized to unity distribution functions $g_{mp}(z)$ of the loop middle monomer unit (monomer unit with the ranking number $M/2$) for the same values of the parameters as in **Figure 7**. For spacer with DP $m = 2$ (**Figure 8a**), all distributions of comblike polymers with n up to 80 collapse on the linear chain distribution ($n = 0$). An increase in m up to 8 (**Figure 8b**) invokes minor deviations of $g_{mp}(z)$ near the grafting surface indicating the onset of changes in the structural organization of the brush. In **SI** we consider the limiting case of loose side chain grafting depicted in **Figure S2**: a single side chain with DP n attached to the middle monomer unit of the loop ($m = M/2$). It is demonstrated in SI (Appendix 3) how increasing n modifies the molecular potential (**Figure S3**) and distribution of the end-points (**Figure S6**), leading first to stratification of the loops into strongly and weakly stretched populations, and subsequently to the development of an extended dead zone near the surface. A similar behavior is expected for comblike polymers with few grafted side chains with DP $n \ll m$. Notably, the parabolic approximation for $U(z)$ in eq 2 does not work in such systems, and in the following we focus on comblike polymers with densely grafted side chains for which eqs 2 and 3 are applicable.

3.2.1 Fraction of bridges X_{comb} in SS-SCF model

Adopting the theoretical model depicted in **Figure 3b**, we consider brushes of loops and bridges formed by comblike polymers with long backbones. Similarly to loops of linear chains, we cut each loop of comblike polymer into two equal subchains with DP N each, and pin middle monomer units of bridges at the symmetry plane between apposing brushes. Substitution of loops by equivalent subchains leads to only minor variations in the molecular potential $U(z)$ (see **Figure S1** in **SI)**, and in the following calculation of fraction X_{comb} of bridges we use $U(z)$ for the brush of tethered by one end comblike subchains (eq 2).

As it has been demonstrated in our previous publication,[36] in solvent-free brushes of comblike polymers the trajectories of backbones with DP M approach the trajectories of linear chains with same DP upon increasing M. The trajectory of the linear chain[38] with DP M and end-point position z_{end} specifies position z_j of monomer unit with ranking number j as

$$\frac{z_j}{z_{end}} = \sin\left(\frac{\pi j}{2M}\right), \quad j = 1, 2, ...M$$

and exhibits the stretching function

$$E = \frac{dz_j}{dj} = \frac{\pi}{2M}\sqrt{z_{end}^2 - z^2}$$

The similarity between trajectories of the backbones of comblike polymers and trajectories of linear chains allows us to relate position z_i of i-th branching unit in comblike polymer with end-point position z_P of the backbone as

$$\frac{z_i}{z_P} \approx \sin\left(\frac{\pi i}{2P}\right), \quad i = 1, 2, ..., P$$

and to introduce the stretching function E_{bb} of the backbone as

$$E_{bb}(z_P, z) = \frac{\pi}{2M}\sqrt{z_P^2 - z^2}$$

The elastic free energy of the backbone is then formulated as

$$\frac{F_{bb}(z_P)}{k_B T} = \frac{3}{2lb}\int_0^{z_P} E_{bb}(z_P, z)dz = \frac{3\pi^2}{16lb}\frac{z_P^2}{M} \tag{18}$$

In total $P = M/m$ side chains with DP n each are exposed to the same molecular potential specified in Eq 2. Zero tension at the free end of each side chain is taken into account to find the end-point position of i-th side chain ($i = 1, 2,...P$) as $z_i/\cos(\kappa n)$. The stretching function $E_{sc,i}(z_i, z)$ of i-th side chain is then given by

$$E_{sc,i}(z_i, z) = \kappa\sqrt{\frac{z_i^2}{\cos^2(\kappa n)} - z^2}$$

The elastic free energy of i-th side chains yields

$$\frac{F_{sc,i}}{k_B T} = \frac{3}{2lb}\int_{z_i}^{z_i/\cos(\kappa n)} E_{sc,i}(z_i, z)dz = \frac{3}{4lb}\kappa z_i^2\left[(\kappa n)(1 + \tan^2(\kappa n)) - \tan(\kappa n)\right] \approx$$

$$\approx \frac{z_i^2}{2lbn}(\kappa n)^4 \quad \text{if} \quad \kappa n \ll 1.$$

By performing summation over $1 \leq i \leq P$, one finds the total elastic free energy of side chains (see **SI** for details),

$$\frac{F_{sc}(z_P)}{k_B T} \approx \frac{1}{4lb}\frac{z_P^2}{M}\left(\frac{m}{n}\right)P^2(\kappa n)^4 = \frac{\pi^4}{64}\frac{z_P^2}{lbM}\left(\frac{n}{m}\right)^3\frac{\eta^4}{P^2(1 + n/m)^4}$$

By implementing the topological ratio η for comblike polymer with long backbone (eq 4 at $q = 1$), $\eta = \sqrt{1 + n/m}$, one finds

$$\frac{F_{sc}(z_P)}{k_BT} = \frac{\pi^4}{64}\frac{z_P^2}{lbM}\left(\frac{n}{m}\right)^3 \frac{1}{P^2(1+n/m)^2} \approx \frac{\pi^4}{64}\frac{z_P^2}{lbM}\left(\frac{n}{m}\right)\frac{1}{P^2} \quad \text{if} \quad n \gg m \tag{19}$$

The ratio of two contributions,

$$\frac{F_{sc}(z_P)}{F_{bb}(z_P)} \approx \frac{\pi^2}{12}\frac{n}{mP^2} = \frac{\pi^2}{12}\frac{nm}{M^2}$$

rapidly decreases upon an increase in length M of the backbone. Therefore, in the limit of long comblike polymers with $M \gg (nm)^{1/2}$, the elastic stretching of side chains in the parabolic potential $U(z)$ (eq 2 with κ specified in eq 3) can be neglected, and the side chains can be considered as almost unperturbed Gaussian coils to support the conjecture that the backbones are "floating in the sea of side chains". Moreover, the relative extension of the architecture-induced dead zone emerging near the grafting surface, and its effect on the elastic free energy of comblike polymer also decrease upon an increase in M, improving eligibility of the parabolic potential in eq 2.

The distribution function $g_{comb}(z_P)$ of the backbone end-points of subchains is similar to the distribution function $g(z_{end})$ of the free ends of linear chains.[36] Therefore, the elastic free energy per molecule in an individual solvent-free brush of comblike polymers with long backbones can be approximated (see **SI**) as

$$\frac{F_{el,comb}(0)}{k_BT} \approx \frac{\pi^2}{8}\frac{D^2}{lbM} = \frac{\pi^2}{8}\eta^2\frac{D^2}{lbN} \tag{20}$$

Within the approximation of unperturbed side chains, thickness h of the boundary layer is still related to thickness $D = \upsilon N/s$ of the brush by eq 5. To account for bridging between apposing brushes of comblike polymers, we substitute eq 20 in eq 6 to formulate

$$\frac{F_{el,comb}(X)}{k_BT} = \frac{\pi^2}{8}\frac{D^2}{lbM}\left[(1-\tau X)^3 + \frac{12X^2}{\pi^2}\right] \tag{21}$$

Minimization of $F_{comb} = F_{el,comb} + F_{mix}$ with respect to X provides the equilibrium fraction of bridges $X_{B,comb}$,

$$\frac{1-X_{B,comb}}{X_{B,comb}} = \left(1 + \frac{9D^2}{\pi^2 lbM}\right)^{1/3} = \left(1 + \frac{9D^2}{\pi^2 lbN}\eta^2\right)^{1/3} = \left(1 + \frac{9N\upsilon^2}{\pi^2 lbs^2}\eta^2\right)^{1/3}, \tag{22}$$

or, equivalently,

$$X_{B,comb} = \frac{1}{1 + \left(1 + \frac{9Nv^2}{\pi^2 lbs^2}\eta^2\right)^{1/3}} \sim$$

$$(F_{el,comb}(0)/k_BT)^{-1/3} = \left(\frac{F_{el,lin}(0)\eta^2}{k_BT}\right)^{-1/3} \quad \text{if} \quad \frac{D^2}{lbM} \gg 1 \qquad (23)$$

Here

$$F_{el,lin}(0) = \frac{\pi^2}{8}\frac{D^2}{lbN}$$

is the elastic free energy per molecule in a dry brush of linear chains with DP N. As it follows from eq 23, within the approximation of unperturbed side chains fraction of bridges $X_{B,comb} \sim \eta^{-2/3}$ decreases compared to that in the brush of linear molecules with the same grafting area $2s$ and DP $2N$. If, however, the elastic free energies of the backbones and of linear chains in the brushes are equal, then according to eqs 22 and 23, fraction of bridges is expected to be the same in both systems (i.e., $X_B = X_{B,comb}$). Recall that these predictions are expected to hold for comblike polymers with $n/m \gg 1$, and long backbones ($M \gg \sqrt{mn}$) exhibiting linear (Gaussian) elasticity.

3.2.2 Fraction of bridges X_{comb} in SF-SCF numerical model

To check the predictions of the analytical SS-SCF theory we performed the numerical SF-SCF calculations for brushes of comblike polymers with different lengths of backbone ($2M$), side chain (n), and spacer (m). Total DP of these polymers equals $N = 2M(1 + n/m)$

In **Figure 9** we present the equilibrium fraction $X_{B,comb}$ of bridges as a function of the sublayer thickness $2D/a = Na^2/s$ for two sets of comblike polymers with fixed backbone DP $2M = 201$, and varied values of n (a) and m (b). As it is seen in **Figures 10**, branched polymers form smaller fraction of bridges compared with linear counterparts with the same DP of the backbone: all the SF-SCF data for comblike polymers is located below the curve with $n = 0$ corresponding to linear chains ("bare backbone").

In **Figures 10** and **Figure 11** we present the results of SF-SCF calculations for the equilibrium fraction of bridges, $X_{B,comb}$, in brushes of comblike polymers with longer backbone, $2M = 1001$, fixed $2D/a = 300$, and varied values of n and m. The SF-SCF data are indicated by symbols, lines are guide for eye. In **Figure 10**, $n = 0$ corresponds to liner chains with $X_B \approx 0.195$, while comblike polymers are found for the values of parameters $n > m$. In accord with the analytical model predicting independence of $X_{B,comb}$ on the molecular parameters, n and m, at fixed values of D and M (eq 23), the

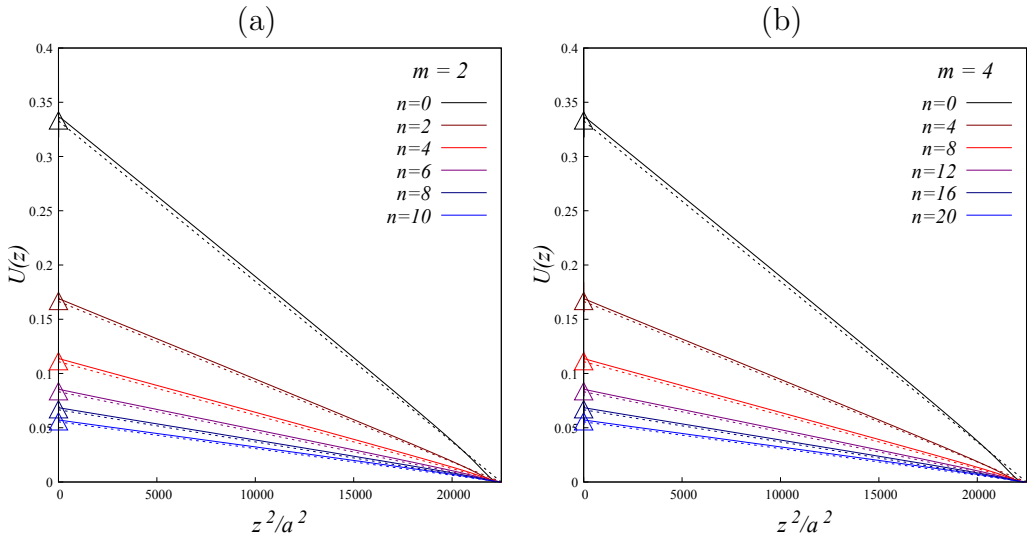

Figure 6: Numerically calculated SF-SCF molecular potential $U(z)/k_BT$ in solvent-free brush of loops as a function of z^2/a^2 for (a) $m = 2$ and (b) $m = 4$ at fixed $2D/a = 300$ and $2M = 1001$, and varying n. Dashed lines indicate ideal parabolas. Theoretical SS-SCF values of $U(0)/(k_BT) = (3\pi/8)(D/2aN)^2 \cdot (1 + n/m)^{-1}$ are shown by triangles on y-axis. Deviations from parabolic shape due to onset of nonlinear elasticity for linear chains ($n = 0$) decrease upon increasing n. As predicted, lines in panel (b) perfectly match lines in panel (a) at equal ratios of n/m (indicated by the same colors).

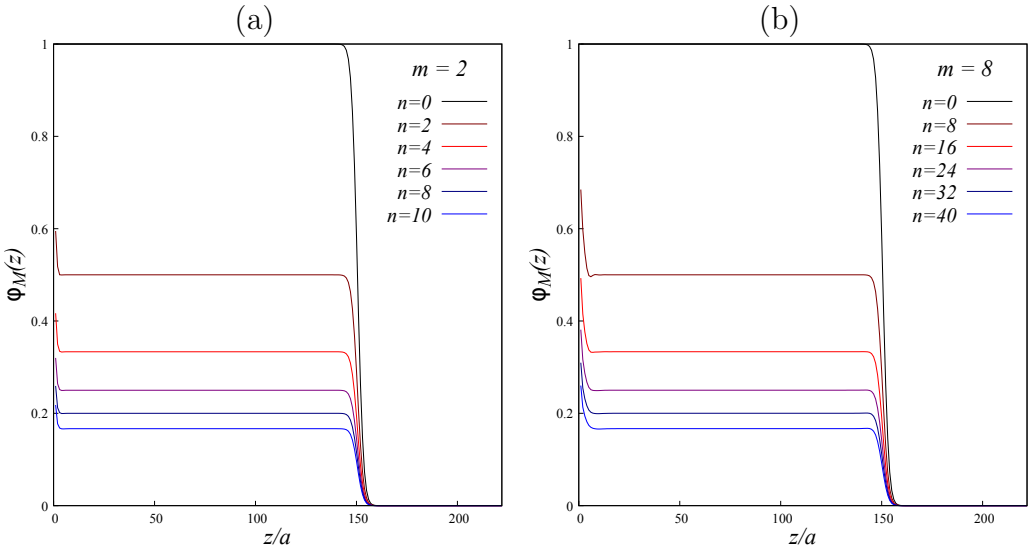

Figure 7: Numerically calculated SF-SCF volume fraction profiles $\varphi_M(z)$ of the backbone monomer units as a function of distance z/a from grafting surface in apposing brushes. $2D = 300$, $2M = 1001$, $m = 2$ (a) and $m = 8$ (b), n varies from 0 to 40.

deviations of $X_{B,comb}$ from X_B are small ($\lesssim 2\%$) for densely grafted combs with $m = 4$, and 8, and slightly increase upon increasing m.

In **Figure 11**, $X_{B,comb}$ is presented as a function of spacer length m. Here, all comblike polymers with densely grafted side chains ($m < 10$) demonstrate fraction of bridges quite close to $X_B \approx 0.195$ for linear chains. However, relative deviation, $(X_B - X_{B,comb})/X_B$, remains below 10% for macromolecules with $n > m$.

As it follows from **Figures 10 and 11**, fraction $X_{B,comb}$ of bridges formed by comblike polymers is fairly described by the analytical SS-SCF model when the spacers and the side chains are relatively small. However, an increase in n and/or m leads to conformational re-arrangements of loops in dry brushes of comblike polymers (see volume fraction profiles in **Figures 5 and 7**) that are absent for linear chains and disregarded in the SS-SCF formalism.

The decrease in stretching of the loop backbones at almost unchanged stretching of the bridges increases the difference in the loop and bridge elastic free energies, and decreases thereby the equilibrium fraction $X_{B,comb}$ of bridges. However, at relatively small values of m and moderate n, a conjecture that conformations of backbones in loops and bridges in B-domain are similar to those of linear counterparts in a "sea of almost unperturbed

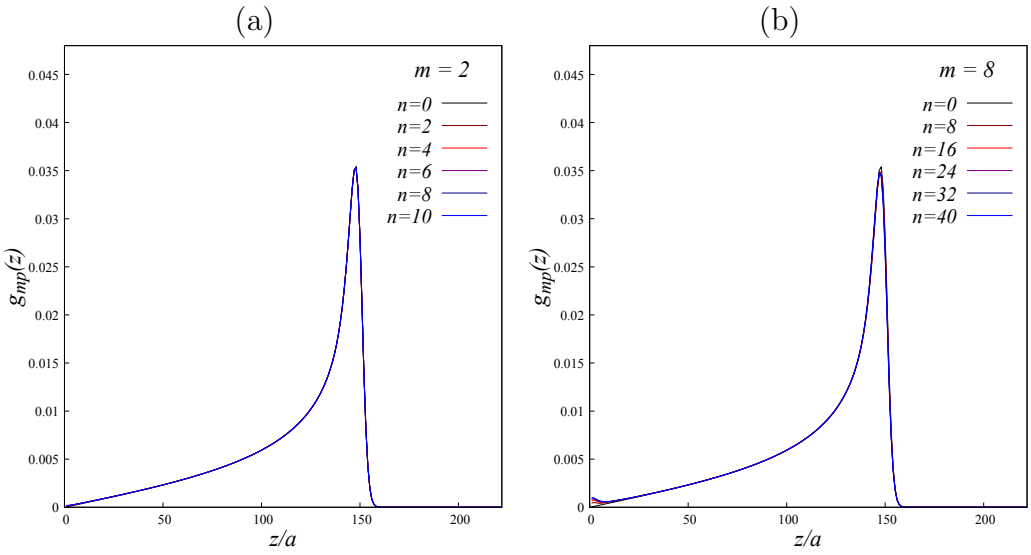

Figure 8: Numerically calculated SF-SCF distributions $g_{mp}(z)$ of backbone middle points (normalized to unity) as a function of distance z/a from grafting surface in each of apposing solvent-free brushes. $2D/a = 300$, $2M = 1001$, $m = 2$ (a), and $m = 8$ (b), n varies from 0 to 80. All curves in panel (a) collapse on top of each other starting from $n = 0$, in panel (b) minor deviations emerge near the grafting surface, indicating onset of bimodal distribution of loops.

side chains" can be viewed as an adequate approximation supported by the numerical SF-SCF modelling. Below we use this approximation (eqs 24 and 23) to estimate the fraction of bridges in lamellae of microphase segregated triblock copolymers with comblike central block.

4 Lamellar mesophase: bridging and shear modulus

The analytical SS-SCF treatment of bridging allows us to estimate the equilibrium fraction of bridges in lamellae formed by ABA copolymer with long A and B blocks (i.e., in the strong segregation limit) from the equilibrium parameters of lamellae formed by diblock $AB/2$ copolymers. The equilibrium structure of microphase segregated lamellae formed by diblock copolymers AB with comblike blocks was analyzed by us previously,[35] and we reproduce here the results that are necessary to estimate the equilibrium fraction $X_{B,1}$ of bridging B-blocks. (Here and below subscript 1 indicates lamellar phase).

Assuming (for simplicity) that molecular parameters of monomer units A and B are similar ($\upsilon_A = \upsilon_B = \upsilon$, $l_A = l_B = l$, $b_A = b_B = b$), one finds the elastic free energy per B-subchain with DP $N_B/2$,

$$\frac{F_B}{k_BT} \approx \frac{\pi^2}{4}\eta_B^2\frac{D_B^2}{lbN_B}, \qquad N_B \gg 1 \tag{24}$$

while the elastic free energy of A-block yields

$$\frac{F_A}{k_BT} \approx \frac{\pi^2}{8}\eta_A^2\frac{D_A^2}{lbN_A}, \qquad N_A \gg 1 \tag{25}$$

with $D_A = \upsilon N_A/s$ and $D_B = \upsilon N_B/(2s)$. For linear A-block $\eta_A = 1$, for branched A-block $\eta_A > 1$.

The elastic free energies of the blocks, $F_B + F_A$, are balanced with the surface free energy of A/B interface,

$$F_{A/B} = \gamma s = \frac{\gamma\upsilon N_A}{D_A} = \frac{\gamma\upsilon N_B}{D_B} \tag{26}$$

with surface tension γ accounting for unfavorable A/B contacts and conformational losses of the blocks in the interfacial layer with thickness $D_{A/B} \ll D_A$, D_B.

By substituting area s per chain from eq 26 in eqs 24, 25, and minimizing the free energy per chain,

$$F = F_A + F_B + F_{A/B}$$

with respect to s (see also ref[35] for lamellae with unequal parameters of A and B monomer units), one finds the equilibrium interfacial area s_1 per diblock copolymer $AB/2$ in the lamellar phase as

$$s_1 = \left(\frac{\pi^2 l \upsilon^2}{8\gamma b}\right)^{1/3} (2\eta_A^2 N_A + \eta_B^2 N_B)^{1/3} \tag{27}$$

and half thickness, $D_{B,1}$, of lamellar B-layer,

$$D_{B,1} = \frac{N_B \upsilon}{2s_1} = \left(\frac{\gamma b \upsilon}{\pi^2 l}\right)^{1/3} \frac{N_B}{(2\eta_A^2 N_A + \eta_B^2 N_B)^{1/3}} \tag{28}$$

and half thickness $D_{A,1} = D_{B,1} N_A / N_B$ of lamellar A-layer. Presumed Gaussian elasticity of the backbones, which is the case at $D_{A,1}/lN_A = D_{B,1}/lN_B \leq 0.5$ imposes limitations for the molecular parameters of the blocks, $2\eta_A^2 N_A + \eta_B^2 N_B \geq (8/\pi^2)\gamma b \upsilon / l^4$ which reduces to 20 for typical values of the parameters, $\gamma = 0.4, b = 18\mathring{A}, l = 2.5\mathring{A}, v = 140\mathring{A}^3$

Eq 27 allows us to estimate the equilibrium fraction $X_{B,1}$ of bridges in B-layers by using eq 23,

$$X_{B,1} = \frac{1}{1 + \left(1 + 2\frac{9D_{B,1}^2}{\pi^2 l b N_B}\eta_B^2\right)^{1/3}} =$$

$$= \frac{1}{1 + \left[1 + \left(\frac{2}{\pi}\right)^{4/3}\left(\frac{9}{\pi^2}\right)\left(\frac{\gamma^{2/3}\upsilon^{2/3}}{l^{5/3}b^{1/3}}\right) N_A^{1/3}\eta_A^{1/3}\frac{x\eta_B^2}{(1+x\eta_B^2)^{2/3}}\right]^{1/3}} \tag{29}$$

with $x = N_B/(2N_A)$. For strongly stretched loops of B-blocks with $\frac{D_{B,1}^2}{lbN_B}\eta_B^2 \gg 1$,

$$X_{B,1} \approx \left(\frac{\pi^2}{18}\frac{lb}{\upsilon^2 N_B \eta_B^2} s_1^2\right)^{1/3} \simeq \left(\frac{l^{5/3}b^{1/3}}{\gamma^{2/3}\upsilon 2/3}\right)^{1/3} \frac{(2\eta_A^2 N_A + \eta_B^2 N_B)^{2/9}}{(N_B \eta_B^2)^{1/3}} \tag{30}$$

Eq 30 specifies how the equilibrium fraction $X_{B,1}$ of bridges in B-layers in microphase segregated lamellae can be manipulated by the molecular parameters of ABA copolymer. Although the expression in eq 30 is asymptotic (obtained in the limit N_A, $N_B \to \infty$), it nonetheless provides important guidelines to mediate the equilibrium fraction $X_{B,1}$ of bridges in microphase segregated lamellae. Notably, while B-blocks are assumed to be comblike polymers, the architecture of A-blocks is not specified in eq 30 (i.e., A-blocks could be linear, comblike, starlike, dendronized, etc.), and the type of their branching is accounted via the topological ratio $\eta_A \geq 1$.

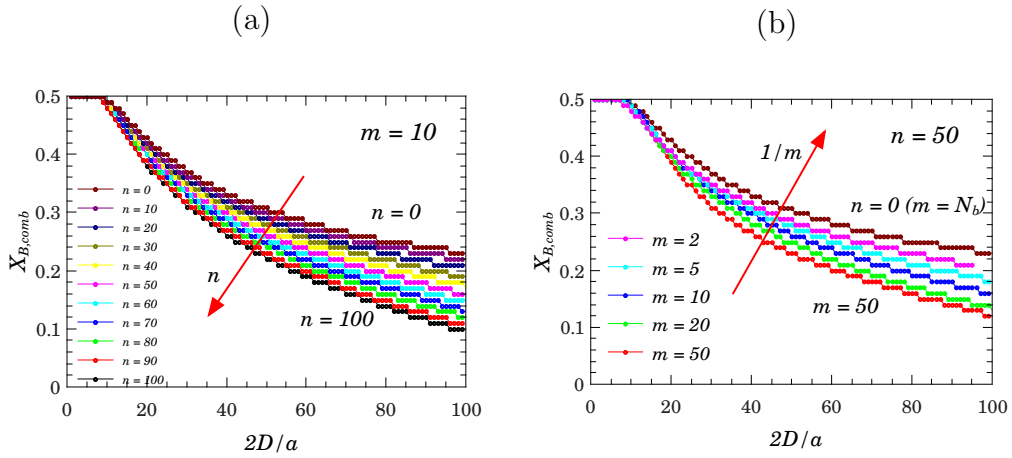

Figure 9: Equilibrium fraction of bridges $X_{B,comb}$ as a function of half distance $2D/a$ between grafting surfaces (sublayer thickness) for constant DP of the main chain $2M = 201$ and varied side chain length n (a) or varied spacer length m (b)

As it follows from eq 30, the equilibrium fraction of bridges $X_{B,1}$ can be manipulated by variations in DPs, N_A and N_B, of the blocks as well as their architectures. In particular, branching of the central (B) or of all of the blocks in ABA copolymer leads to the decrease in $X_{B,1}$ compared to ABA triblock with linear blocks of similar DPs. Symmetric comblike branching of A and B blocks leads to a stronger decrease in $X_{B,1}$ compared with triblock with branched B and linear blocks A. Branching of A-blocks with $\eta_A > \eta_B$ increases $X_{B,1}$ compared to that for linear A-block.

In **Figure 12** we present $X_{B,1}$ calculated according to eq 29 as a function of copolymer composition $f_B = N_B/(2N_A + N_B)$ for various values of η_B. Solid and dotted lines indicate stable and metastable states of the lamellar morphology. The crossovers between solid and dotted lines (indicated by arrows) correspond to morphological transitions from lamellae to cylinders with A-domains in B-matrix at $\eta_B = 2$ and $\eta_B = 5$. For linear B-blocks with $\eta_B = 1$, lamellae transform in inverted cylinders with B-domains in A-matrix at small values of f_B. For comblike B-blocks with $\eta_B > 1$, the transition to cylinders is shifted towards smaller values of f_B,[35] decreasing the range of stability of the lamellar phase.

4.0.1 Shear modulus G

Fraction $X_{B,1}$ of bridging B-chains governs the shear modulus G of microphase segregated melt with lamellar morphology. It characterizes the

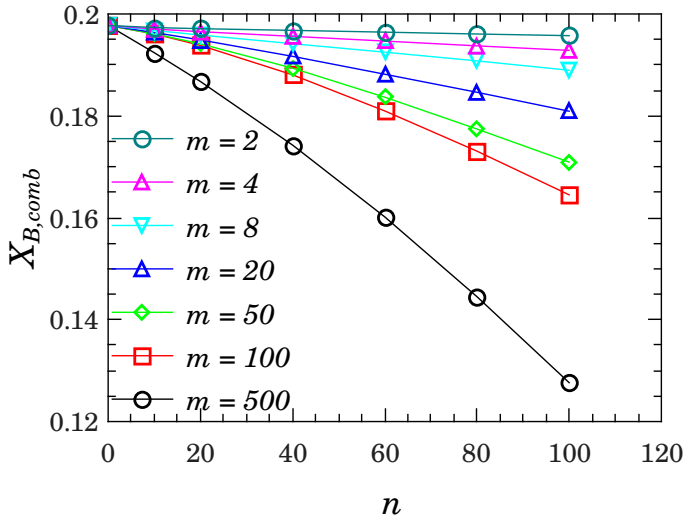

Figure 10: Equilibrium fraction of bridges $X_{B,comb}$ as a function of side chains length n for $2M = 1001$, $2D/a = 300$.

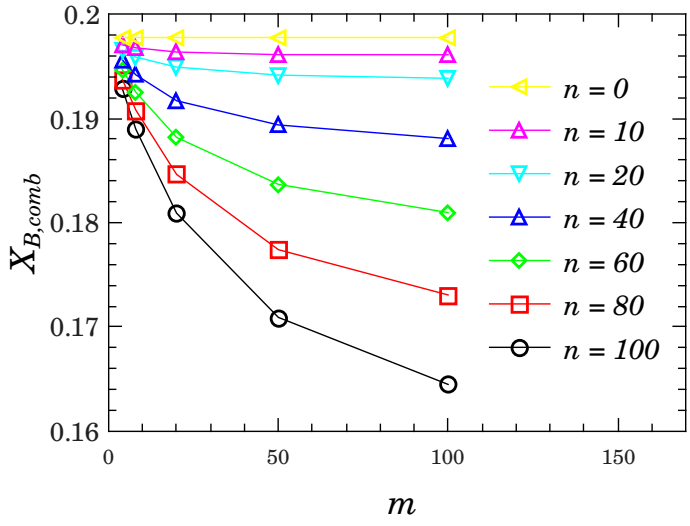

Figure 11: Equilibrium fraction of bridges $X_{B,comb}$ as a function of spacer length m for $2M = 1001$, $2D/a = 300$.

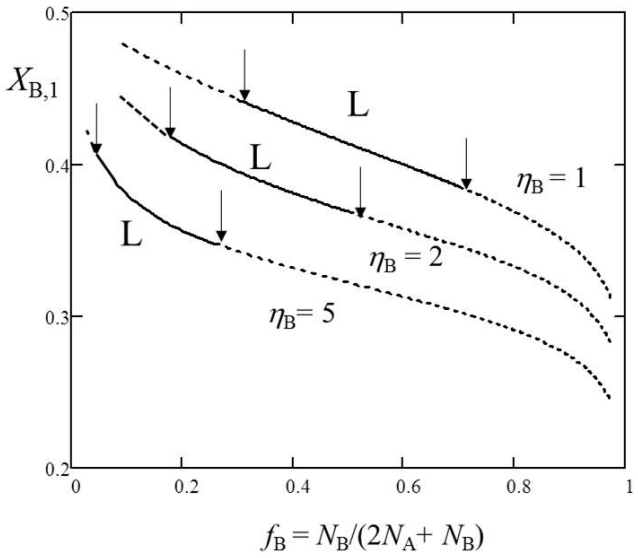

Figure 12: Fraction $X_{B,1}$ of bridging B-blocks in lamellae as a function of $f_B = N_B/(2N_A+N_B)$, $N_A = 200$. Dotted lines indicate metastable states: at these compositions nonplanar (cylindrical, spherical) morphologies are thermodynamically more favorable. Arrows indicate bounds of thermodynamic stability of lamellar phase.

relative lateral displacement of the lamellae due to applied force acting along the lamellar plane. The backbones of bridging comblike B-blocks exhibit the Gaussian elasticity in lateral direction, and the lateral displacement 2Δ of the upper A/B boundary with respect to the lower A/B boundary of the B-layer is opposed by the restoring elastic force,

$$\sigma = k_B T \frac{3\Delta}{lbM_B} \frac{X_{B,1}}{s_1},$$

per unit area of interface to counteract the applied stress. Here M_B is half of DP of the backbone of B-block.

The equilibrium shear modulus $G = \sigma/\varepsilon$ defined as the coefficient between stress σ and strain $\varepsilon = \Delta/D_{B,1}$ is then given by

$$\frac{G}{k_B T} = 3\frac{\upsilon N_B}{lbs_1^2 M_B} X_{B,1} = 3\frac{\upsilon}{lbs_1^2}\eta_B^2 X_{B,1} \tag{31}$$

By substituting s_1 from eq 27, and $X_{B,1}$ from eq 30 in eq 31, one predicts the shear modulus G of a perfectly aligned stack of lamellae,

$$\frac{\upsilon G}{k_B T} = 3\frac{\eta_B^2}{N_A^{2/3}(1+x\eta_B^2)^{2/3}} \frac{C}{\left[1+\left(1+(9/\pi^2)\, C N_A^{1/3}\eta_A^{1/3} x\eta_B^2/(1+x\eta_B^2)^{2/3}\right)^{1/3}\right]} \tag{32}$$

with dimensionless constant

$$C = \left(\frac{2}{\pi}\right)^{4/3} \frac{\gamma^{2/3}\upsilon^{2/3}}{l^{5/3}b^{1/3}}$$

For typical flexible polymers, $b \simeq \upsilon^{1/3}$, $\gamma \simeq 1$, leading to $C \simeq 1$.

Eqs 31 and 32 presume linear backbone elasticity leading to equal and independent of deformation partitioning of monomer units along vertical to the interface (z), and two lateral directions. Nonlinear elasticity of strongly stretched backbones approaching fully stretched states, leads to re-distribution of monomer units in favor of vertical direction, decreasing the fraction of shear-responsive monomer units and increasing shear modulus G. Therefore eqs 31 and 32 provide lower boundary for G in lamellae with strongly stretched backbone of central block B. An increase in elastic moduli due to nonlinear elasticity of strongly stretched backbones was detected and rationalized earlier in self-assembled networks of ABA block copolymers with comblike central block.[42] This non-linear effect will be considered by us in a separate forthcoming publication.

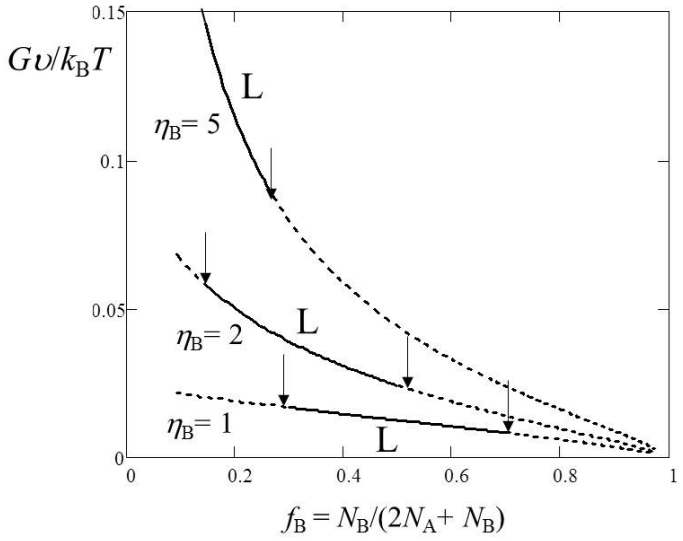

Figure 13: Shear modulus $G\upsilon/(k_BT)$ as a function of $f_B = N_B/(2N_A + N_B)$. Dotted lines indicate metastable states of lamellae. Arrows indicate bounds of thermodynamic stability of lamellar phase.

In **Figure 13**, we present normalized shear modulus $\upsilon G/k_BT$ as a function of copolymer composition $f_B = N_B/(2N_A + N_B)$ for fixed DP $N_A = 200$ and various degrees of branching of the central B-block (i.e., upon an increase in η_B at fixed DP N_B). As in **Figure 13**, arrows at the crossovers of solid and dashed lines indicate the lost of stabilty of the lamellar phase in favour of cylinders. Although the equilibrium fraction $X_{B,1}$ of bridges between A/B interfaces decreases upon an increase in η_B, the shear modulus G increases upon branching of B-blocks (i.e., upon increasing η_B). This is because branching of B-block at fixed DP N_B decreases the length $M_B = N_B/\eta_B^2$ of the backbone, and larger stress $\sigma \sim M_B^{-1}$ must be applied to laterally displace the lamellar layers.

5 Conclusions

In this study we have theoretically examined the equilibrium properties of solvent-free planar brushes formed by loops and bridges of comblike polymers. We focussed on the effect of architecture of the tethered chains on the equilibrium fraction of bridges connecting apposing grafting surfaces. Such layers model the lamellae formed in micrpophase segregated melts of ABA

block copolymers, and we aimed to analyze how fraction of bridges depends on the architectural parameters of the blocks. The applied analytical SS-SCF model presumed: (i) local flexibility of the side and main chains, (ii) the Gaussian elasticity of macromolecules on all length scales, and (iii) lack of brush stratification that leads to architecture-induced dead zones.

We demonstrated that in the parabolic potential framework, fraction $X_{B,1}$ of bridges formed by central B-block of ABA triblock copolymer can be estimated from the equilibrium properties of lamellae formed by diblock $AB/2$ block copolymer. In this approach, B-loop is modelled as two subchains with DP $N_B/2$, while the middle point of B-bridge is fixed at the boundary of Wigner-Seitz cell. The numerical SF-SCF calculations performed for solvent-free planar layers formed by loops and bridges of linear and comblike polymers were in accord with the analytical SS-SCF model in eligible ranges of the system parameters.

As we have shown, an increase in the degree of branching of the B-block leads to a decrease in the fraction of bridges with a concomitant increase in the shear modulus. Thus the results of our study prove the possibility to control mechanical properties of the lamellar mesophases of ABA triblock copolymers by tuning architecture of both central and terminal blocks. In particular, we demonstrated that replacement of the central linear B-block by the comblike one (with the same DP) allows to increase the shear modulus of the material.

Notably, strong branching of B-blocks destabilizes the lamellar phase (matastable states are indicated by dotted lines in **Figure 12**), leading to morphological transitions into cylinders, and subsequently to spheres. We will consider these morphologies in our forthcoming publication.

Associated Content

Supporting Information: Description of the numerical SF-SCF method and computational algorithm. Analytical calculation of elastic free energies of the main chain and side chains of comblike polymer in a planar brush. Structural and thermodynamic properties of the brush formed by loops with single side chain calculated by the SF-SCF method.

Acknowledgment

This work was supported by Ministry of Research and Education of the Russian Federation within State Contract N 14.W03.31.0022.

References

[1] Pickett G. T. Classical Path Analysis of end-Grafted Dendrimers: Dendrimer Forest. *Macromolecules* **2001**, *34*, 8784–8791

[2] Kröger M.; Peleg O.; Halperin A. From Dendrimers to Dendronized Polymers and Forests: Scaling Theory and its Limitations. *Macromolecules* **2010**, *43*, 6213–6224.

[3] Gergidis L. N.; Kalogirou A.; Vlahos C. Dendritic Brushes under Good Solvent Conditions: A Simulation Study. *Langmuir* **2012**, *28*, 17176–17185.

[4] Polotsky, A.A.; Gillich, T.; Borisov, O.V.; Leermakers, F.A.M.; Textor, M.; Birshtein, T.M. Dendritic versus Linear Polymer Brushes: Self-Consistent Field Modelling, Scaling Theory, and Experiment. *Macromolecules* **2010**, *43* 9555–9566

[5] Borisov, O. V. ; Polotsky, A. A.; Rud, O. V.; Zhulina, E. B.; Leermakers, F. A. M.; Birshtein, T. M. Dendron Brushes and Dendronized Polymers: A Theoretical Outlook. *Soft Matter* **2014**, *10*, 2093–2101.

[6] Li, C.-W.; Merlitz, H.; Wu, C.-X.; Sommer, J.-U. The structure of brushes made of dendrimers: Recent Advances *Polymer* **2016**, *98*, 437–447

[7] Leermakers, F. A. M. ; Zhulina, E. B. ; Borisov, O.V. Interaction forces and lubrication of dendronized surfaces *Current Opinion in Colloid and Interface Science***2017**, *27*, 50–56

[8] Wurm, F.; Frey, H. Linear-dendritic block copolymers: the state of the art and exciting perspectives *Progress in Polymer Science* **2011**, *36*, 1–52

[9] Blasco, E.; Pinol, M.; Oriol, L. Responsive Linear-Dendritic Block Copolymers *Macromolecular Rapid Communications,* **2014**, *35(12)*, 1090–1115

[10] Garcia-Juan H.; Nogales, A.; Blasco, E.; Martinez, J.C.; Sics, I.; Ezquerra T.A.; Pinol, M.; Oriol, L. Self-assembly of thermo and light responsive amphiphilic linear dendritic block copolymers *European Polymer Journal* **2016**, *81*, 621–633

[11] Mirsharghi S.; Knudsen, K.D.; Bagherifam, S.; Niström, B.; Boas, U. Preparation and self-assembly of amphiphilic polylysine dendrons *New J.Chem.* **2016**, *40*, 3597–3611

[12] Fan, X.; Zhao, Y.; Xu, W.; Li, L. Linear-Dendritic Block Copolymer for Drug and Gene Delivery. *Mater.Sci.Eng.C* **2016**, *62*, 943–959

[13] J. Rzayev Synthethis of polystyrene-polylactide bottlebrush block copolymers and their melt self-assembly into large domain nanostructures. *Macromolecules* **2009**, *42*, 2135–2141

[14] Liberman-Martin, A.L.; Chu, C.K.; Grubbs, R.H. Application of Bottlebrush Block Copolymers as Photonic Crystals. *Macromol.Rapid.Comm.* **2017**, *38*, 1700058

[15] Song, D.P.; Zhao, T.H.; Guidetti, G.; Vignolini, S.; Parker, R.M. Hierarchical Photonic Pigments via the Confined Self-Assembly of Bottlebrush Block Copolymers. *ACS Nano* **2019**, *13*, 1764–1771.

[16] J. Bolton, T.S. Baile, J. Rzayev. Large pore size nanoporous materials from self-assembly of asymmetric bottlebrush block copolymers. *Nano Lett.* **2011**, *11*, 998–1001

[17] Y. Gai, D.-P. Song, B. M. Yavitt, J. J. Watkins. Polystyrene-block-poly(ethylene oxide) Bottlebrush Block CopolymerMorphology Transitions: Influence of Side Chain Length and Volume Fraction. *Macromolecules* **2017**, *50*, 1503–1511

[18] M.B. Runge, N.B. Bowden. Synthesis of High Molecular Weight Comb Block Copolymers and Their Assembly into Ordered Morphologies in the Solid State. *JACS* **2007**, *129*, 10551–10560

[19] M.B. Runge, C.E. Lipscomb, L.R. Ditzler, M.K. Mahanthappa, A.V. Tivanski, N.B. Bowden. Investigation of the Assembly of Comb Block Copolymers in the Solid State. *Macromolecules* **2008**, *41*, 7687–7694

[20] H.-F. Fei, B. M. Yavitt, X. Hu, G. Kopanati, A. Ribbe, J. J. Watkins.Influence of Molecular Architecture and Chain Flexibility on the Phase Map of Polystyrene-block-poly(dimethylsiloxane) Brush Block Copolymers. *Macromolecules* **2019**, *52*, 6449–6457

[21] D.F. Sunday, A. B. Chang, C. D. Liman, E. Gann, D. M. Delongchamp, L. Thomsen, M. W. Matsen, R. H. Grubbs, C. L. Soles. Self-Assembly of ABC Bottlebrush Triblock Terpolymers with Evidence for Looped Backbone Conformations. *Macromolecules* **2018**, *51*(4), 1557–1566

[22] J. Bolton, J. Rzayev. Synthesis and Melt Self-Assembly of PS-PMMA-PLA Triblock Bottlebrush Copolymers. *Macromolecules* **2014**, 47, 2864–2874

[23] T. Gillich, Benetti, E. M., Rakhmatullina, E., Konradi, R., Li, W., Zhang, A., Schlüter, A. D., Textor, M. Self-Assembly of Focal Point Oligo-Catechol Ethylene Glycol Dendrons on Titanium Oxide Surfaces: Adsorption Kinetics, Surface Characterization , and Nonfouling Properties *J. Am. Chem. Soc.* **2011**, *133*, 10940–10950.

[24] Yeh, P.Y.J.; Kainthan, R.K.; Zou, Y.; Chiao, M.; Kizhakkedathu, J.N. Self-assembled monothiol-terminated hyperbranched polyglycerols on a gold surface: a comparative study on the structure, morphology, and protein adsorption characteristics with linear poly(ethylene glycol). *Langmuir* **2008**, *24*, 4907–4916.

[25] T. Gillich, Acikgöz C. Isa L., Schlüter, A. D., Spencer N.D. , Textor, M. PEG-Stabilized Core-Shell Nanoparticles: Impact of Linear versus Dendritic Polymer Shell Architecture on Colloidal Properties and the Reversibility of Temperature-Induced Aggregation. *ACS Nano* **2013**, *7*, 316–329.

[26] M. Vatankhah-Varnosfaderani, A.N. Keith, Y. Cong, H. Liang, M. Rosenthal, M. Sztucki, C. Clair, S. Magonov, D.A. Ivanov, A. V. Dobrynin, S.S. Sheiko. Chameleon-like elastomers with molecularly encodded strain-adaptive stiffening and coloration. *Science* **2019**, 359, 1509–1513.

[27] Yuan, J.; Müller, A.H.E.; Matyjaszewski, K.; Sheiko, S. In *Polymer Science: A Comprehensive Reference*; Matyjaszewski, K., Möller, M., Eds.-in-Chief; Elsevier, Amsterdam, 2012.

[28] S. Tu, C. K. Choudhury, I. Luzinov, O. Kuksenok. Recent advances towards applications of molecular bottlebrushes and their conjugates. *Current Opinion in Solid State and Materials Science* **2019**, *23* (1) 50–61

[29] G. Xie, M. R. Martinez, M. Olszewski, S. S. Sheiko, K. Matyjaszewski. Molecular Bottlebrushes as Novel Materials. *Biomacromolecules* **2019**, *20* (1), 27–54

[30] Polotsky, A. A.; Leermakers, F. A. M.; Zhulina, E. B.; Birshtein, T. M. On the Two-Population Structure of Brushes Made of Arm-Grafted Polymer Stars. *Macromolecules* **2012**, *45*, 7260–7273.

[31] Zhulina, E. B.; Leermakers, F. A. M.; Borisov O.V. Theory of brushes formed by Ψ-shaped macromolecules at solid-liquid interfaces. *Langmuir* **2015,***31* (23), 6514–6522

[32] Zhulina, E. B. ; Leermakers, F. A. M.; Borisov O.V. Ideal mixing in multicomponent brushes of branched macromolecules. *Macromolecules* **2015**,*48* (23), 5614–5622

[33] Lebedeva, I.O.; Zhulina, E. B. ; Leermakers, F. A. M.; Borisov O.V. Dendron and Hyperbranched Polymer Brushes in Good and Poor Solvents. *Langmuir* **2017**,*33*, 1315-1325

[34] Zhulina, E. B. ; Leermakers, F. A. M.; Borisov O.V. Brushes of Cycled Macromolecules: Structure and Lubricating Properties. *Macromolecules* **2016**,*49* (22), 8758–8767

[35] E.B. Zhulina, S.S. Sheiko, A.V. Dobrynin, O.V. Borisov. Microphase segregation in the melts of bottlebrush block copolymers. *Macromolecules* **2020**, *53* (7), 2582–2593

[36] Zhulina, E.B.; Mikhailov, I.V.; Borisov, O.V. Brushes and lamellar mesophases of comb-shaped (co)polymers: a self-consistent field theory. *PCCP* **2020**, *22* (40), 23385–23398

[37] Zhulina, E.B.; Halperin, A. Lamellar Mesogels and Mesophases: A Self-Consistent Field Theory. *Macromolecules* **1992**, *25*, 5730–5741

[38] Semenov, A. N. Contribution to the Theory of Microphase Layering in Block-Copolymer Melts. *Sov. Phys. JETP* **1985**, 61, 733–742.

[39] Fleer, G.J.; Cohen Stuart, M.A.; Scheutjens, J.M.H.M.; Cosgrove, T.; Vincent, B. *Polymers at Interfaces*, Chapman & Hall, London, 1993

[40] Levi, A. E.; Lequieu, V; Horne, J. D. ; Bates, M. W. ; Ren, J. M.; Delaney, K.T.; Fredrickson, G. H. ; Bates, C. M.. Miktoarm Stars via Grafting-Through Copolymerization: Self-Assembly and the Star-to-Bottlebrush Transition. *Macromolecules* **2019**, *52*, 1794–1802.

[41] Zhulina, E.B.; Sheiko, S.S. ; Borisov, O.V. Solution and melts of barbwire bottlebrushes: hierarchical structure and scale-dependent elasticity. *Macromolecules* **2019**, *52*, 1671–1684.

[42] Sheiko, S.S.; Dobrynin, A.V. Architectural Code for Rubber Elasticity: From Supersoft to Superfirm Materials. *Macromolecules* **2019**, *52*, 75317546